8-29-2003

Salt modulates the stability and lipid binding affinity of the adipocyte lipid-binding protein

Allyn J. Schoeffler
Louisiana State University

Carmen R. Ruiz
Louisiana State University

Allison M. Joubert
Louisiana State University

Xuemei Yang
Louisiana State University

Vince J. LiCata
Louisiana State University

Recommended Citation

Schoeffler, A., Ruiz, C., Joubert, A., Yang, X., & LiCata, V. (2003). Salt modulates the stability and lipid binding affinity of the adipocyte lipid-binding protein. *Journal of Biological Chemistry, 278* (35), 33268-33275. https://doi.org/10.1074/jbc.M304955200

THE JOURNAL OF BIOLOGICAL CHEMISTRY
Vol. 278, No. 35, Issue of August 29, pp. 33268–33275, 2003
Printed in U.S.A.

Salt Modulates the Stability and Lipid Binding Affinity of the Adipocyte Lipid-binding Protein*

Received for publication, May 12, 2003, and in revised form, June 4, 2003
Published, JBC Papers in Press, June 6, 2003, DOI 10.1074/jbc.M304955200

Allyn J. Schoeffler, Carmen R. Ruiz, Allison M. Joubert, Xuemei Yang, and Vince J. LiCata‡

From the Department of Biological Sciences, Louisiana State University, Baton Rouge, Louisiana 70803

Adipocyte lipid-binding protein (ALBP or aP2) is an intracellular fatty acid-binding protein that is found in adipocytes and macrophages and binds a large variety of intracellular lipids with high affinity. Although intracellular lipids are frequently charged, biochemical studies of lipid-binding proteins and their interactions often focus most heavily on the hydrophobic aspects of these proteins and their interactions. In this study, we have characterized the effects of KCl on the stability and lipid binding properties of ALBP. We find that added salt dramatically stabilizes ALBP, increasing its ΔG of unfolding by 3–5 kcal/mol. At 37 °C salt can more than double the stability of the protein. At the same time, salt inhibits the binding of the fluorescent lipid 1-anilinonaphthalene-8-sulfonate (ANS) to the protein and induces direct displacement of the lipid from the protein. Thermodynamic linkage analysis of the salt inhibition of ANS binding shows a nearly 1:1 reciprocal linkage: *i.e.* one ion is released from ALBP when ANS binds, and *vice versa*. Kinetic experiments show that salt reduces the rate of association between ANS and ALBP while simultaneously increasing the dissociation rate of ANS from the protein. We depict and discuss the thermodynamic linkages among stability, lipid binding, and salt effects for ALBP, including the use of these linkages to calculate the affinity of ANS for the denatured state of ALBP and its dependence on salt concentration. We also discuss the potential molecular origins and potential intracellular consequences of the demonstrated salt linkages to stability and lipid binding in ALBP.

Adipocyte lipid-binding protein (ALBP or aP2)[1] is a member of the intracellular lipid-binding protein (iLBP) family, also known collectively as the intracellular fatty acid-binding proteins. Members of the iLBP family are found in a number of mammalian tissues, including liver, adipose, heart, brain, intestinal, and epithelial tissues (for reviews, see *e.g.* Refs. 1–3). As its name suggests, ALBP is found predominantly in adipocytes, where it constitutes 1–5% of the total soluble protein. In addition, ALBP is found in macrophages, where it has been linked to the development of atherosclerosis (4, 5). ALBP has also been implicated in the development of type II diabetes (6). Like most iLBPs, ALBP can bind a number of fatty acids of at least 14 carbons as well as other hydrophobic ligands with carboxylate or sulfonate moieties in its large, water-filled cavity (reviewed in Ref. 4). ALBP also tightly binds the fluorescent probe 1-anilinonaphthalene-8-sulfonate (ANS) (7, 8). ANS binds specifically in the ALBP lipid binding cavity (see Fig. 1), is a competitive inhibitor of fatty acid binding, and produces a large increase in fluorescence upon binding (7, 8).

Members of the iLBP family share remarkably similar tertiary structures. The iLBP fold consists of a 10-strand antiparallel β-barrel and a helix-turn-helix cap (see Fig. 1). They all possess a ligand binding cavity of ~1000 Å^3 located in the top half of the β-barrel (4). In contrast, the amino acid sequence homology between family members ranges from 23 to 69%, with 39 highly conserved residues (4). In addition, iLBPs each have distinct surface charge potentials (10). ALBP has a nearly hemispherically distributed surface charge potential: mostly positively charged on the top and mostly negatively charged on the bottom (10). The varied charge topologies of the different iLBPs suggest that surface charge may play an important role in differentiating them *in vivo*.

The role that surface charge plays in iLBP function has to date been predominantly characterized in a series of studies by Storch and associates (11–13), which examine the interactions of iLBPs with lipid vesicles. These studies have demonstrated that ALBP transfers a fluorescent fatty acid to negatively charged lipid membranes more rapidly than to neutral or positively charged membranes (12), that the transfer involves direct collision/interaction of ALBP and the vesicle (11, 12), and that salt attenuates the transfer reaction (12). Neutralizing the surface lysines of ALBP by acetylation also inhibits the ability of ALBP to form complexes with anionic vesicles (13). These studies demonstrate that electrostatic attraction is directly involved in the mediation of ALBP-membrane interactions.

In addition to the surface electrostatic topologies and the ALBP-membrane interaction studies mentioned above, a variety of other recent studies support the significance of electrostatic effects in iLBP-lipid and ANS-protein interactions. 1) Mutation of charged residues in the binding cavity of intestinal fatty acid-binding protein can change the lipid binding specificity of the protein (14). 2) The binding of ANS to intestinal fatty acid-binding protein has been observed to be dependent on ionic strength (I) at low NaCl concentrations, and this observation was attributed to an electrostatic screening effect (15). 3) Recent studies of "nonspecific" ANS surface binding to a series of different proteins using titration calorimetry concluded that most ANS molecules bind predominantly via electrostatic association and to a lesser extent via hydrophobic interactions (16). 4) In ANS displacement assays, ALBP has been shown to bind retinoic acid, which has a carboxylate group, with moderate affinity, whereas the protein exhibits negligible affinity for retinol (7). Thus, whereas in one sense it might seem unusual to characterize electrostatic effects on

* This work was supported by NASA Grant NAG 2-1511. The costs of publication of this article were defrayed in part by the payment of page charges. This article must therefore be hereby marked "*advertisement*" in accordance with 18 U.S.C. Section 1734 solely to indicate this fact.

‡ To whom correspondence should be addressed. Tel. 225-578-5233; Fax: 225-578-2597; E-mail: licata@lsu.edu.

[1] The abbreviations used are: ALBP, adipocyte lipid-binding protein; iLBP, intracellular lipid-binding protein; apo-ALBP, ALBP without bound lipid; holo-ALBP, ALBP with bound lipid; ANS, 1-anilinonaphthalene-8-sulfonate.

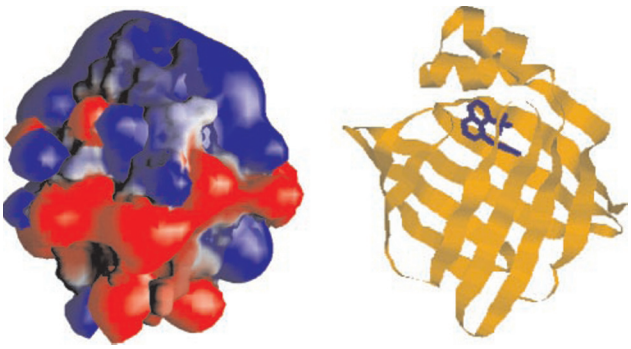

FIG. 1. **Structure and electrostatic surface topology of ALBP.** The *panel* on the *right* shows a *ribbon diagram* of the tertiary structure of ALBP with ANS bound in the lipid binding cavity (Protein Data Bank code 2ANS (8)). The *panel* on the *left* shows the electrostatic surface potential topology of ALBP calculated using the program GRASP (9), as described previously (10). Both depictions of the protein are in the same orientation. In the electrostatic potential depiction, *blue* represents positive potential, *red* is negative potential, and *white* is neutral.

interactions that are frequently considered to be predominantly hydrophobic, it is becoming increasingly clear that electrostatic effects are a major regulator of lipid-protein interactions. This has led us to investigate the effects of salt on ALBP. The results demonstrate and quantitate the regulatory effects of salt on the function and stability of ALBP.

EXPERIMENTAL PROCEDURES

Purification of ALBP—ALBP was purified as described previously (17, 18). The pRSET plasmid for overexpression of murine ALBP was a gift from Dave Bernlohr at the University of Minnesota. An extinction coefficient of 15,500 M^{-1} cm^{-1} was used to determine protein concentrations (19). Protein was stored at −70 °C until use.

Chemical Denaturations—For chemical denaturation studies, ALBP was first dialyzed extensively against appropriate buffers (10 mM potassium phosphate at pH 7.5, with varying KCl concentrations from 0 to 2 M). Urea stocks were deionized by stirring with AG 501-X8 deionizing resin (5 g/100 ml of solution, obtained from Bio-Rad) for 1 h in water. Urea concentrations were then determined by refractive index as described by Pace (20), and the stocks were incorporated into the appropriate buffers. Stepwise chemical denaturations were performed by incubating individual aliquots of protein at 0.1–0.2 mg/ml with buffered urea for 1 h, well past the time required to reach equilibrium (data not shown). For denaturations of ALBP with ANS bound, 100 μM ANS was included in all experimental buffers. This concentration of ANS is saturating at all salt concentrations examined. Denaturation was monitored by scanning each sample in an Aviv model 202 circular dichroism spectrophotometer from 225 to 213 nm in a quartz cuvette with a 0.2-cm path length.

Reversibility of ALBP unfolding was determined at high (1 M) and low (50 mM) salt concentrations by incubating ALBP in denaturing levels of urea plus salt for 1 h, followed by dialysis to remove the urea. Redenaturation was then performed, and full reversibility (recovery of the same $\Delta G_{unfolding}$) was obtained.

Data Analysis of Denaturation Curves—The raw CD signal (in millidegrees) of each sample at 216, 217, and 218 nm was transformed into molar ellipticity (Δε) (21), and denaturation curves at each wavelength were analyzed using the nonlinear form of the linear extrapolation method (22).

$$\Delta\varepsilon = \frac{(\Delta\varepsilon_N + m_N[D]) + (\Delta\varepsilon_U + m_U[D])\, e^{-(\Delta G^0_{N\rightarrow U}/RT + m_G[D]/RT)}}{1 + e^{-(\Delta G^0_{N\rightarrow U}/RT + m_G[D]/RT)}} \quad \text{(Eq. 1)}$$

Here Δε represents the molar ellipticity at a given wavelength (the dependent variable), [D] is the molar denaturant concentration (the independent variable), $\Delta\epsilon_N$ is the y intercept of the native state base line, m_N is the slope of the native state base line, $\Delta\epsilon_U$ is the y intercept of the unfolded state baseline, m_U is the slope of the unfolded state base line, $\Delta G^0_{N\rightarrow U}$ is the extrapolated free energy of unfolding in the absence of denaturant, R is the gas constant, T is the temperature in Kelvin, and m_G (the "m value") is the slope of the calculated dependence of ΔG on [D]. Data were fit using the program KaleidaGraph (Synergy Software, Inc.).

ANS Binding—The binding of ANS to ALBP was monitored using a FluoroMax-2 fluorometer. ANS concentrations in ethanol were determined using the extinction coefficient 7800 M^{-1} cm^{-1} (Molecular Probes, Inc., Eugene, OR). ANS in buffer plus 1% ethanol was titrated into protein (in 10 mM potassium phosphate, pH 7.5, containing concentrations of KCl as noted) and using protein concentrations near 0.05 μM. Samples were incubated for 2 min with stirring, and then fluorescence was monitored with 5-nm slits and excitation and emission wavelengths of 369 and 470 nm. Fluorescence was corrected for volume increase during the titration. A corresponding titration of the background fluorescence of ANS titrated into buffer was collected and subtracted from each individual binding titration. The resulting fluorescence titrations were analyzed using a single-site binding isotherm,

$$F = (F_{max}*[ANS]/K_d)/(1 + [ANS]/K_d) \quad \text{(Eq. 2)}$$

where F_{max} is the maximum fluorescence obtained upon binding, [ANS] is the concentration of ANS, and K_d is the dissociation constant of ANS from ALBP. This equation assumes that the total concentration of ANS is negligibly different from the free ANS concentration, which is true when $K_d \gg$ [ALBP]. Fits of the isotherms with the lowest (tightest) K_d values using a quadratic solution of the binding polynomial, which does not make this assumption (23–25), yield the same K_d values within error and verify the applicability of Equation 2 to these data. The lowest (tightest) K_d values in this study, at the lowest salt concentrations, are ~10 times higher than the [ALBP]. Data were fit using the program KaleidaGraph.

It should be noted that the ANS binding activity of ALBP is extremely sensitive to storage and preparation conditions, particularly to being stored in dilute form. In all of our experiments, protein was stored at −70 °C at a concentration greater than 3 mg/ml and thawed and diluted immediately before use. Even short periods (*e.g.* 16 h) of incubation in dilute (<10 μM) solution at 4 °C result in a significant loss of binding affinity. In addition, the use of nitrocellulose filters for buffer preparation results in interference in the fluorescence assay. Neither of these problems affects the stability of ALBP.

Salt Linkage Analysis—Linked ion release upon binding of ANS to ALBP was calculated using a basic linkage relationship (26, 27); *e.g.* for KCl, the relationship is as follows.

$$\{\partial \ln 1/K_d\}/\{\partial \ln[KCl]\} = \Delta n_{ions} = \Delta n K^+ + \Delta n Cl^- \quad \text{(Eq. 3)}$$

Thus, a plot of $\ln(1/K_d^{ANS})$ *versus* ln [KCl] will have a slope equivalent to the net number of ions that are bound or released when ANS binds.

Direct Ligand Displacement—To examine the direct displacement of ANS by salt, KCl was titrated into ANS-bound ALBP, and the decrease in fluorescence as ANS was released was recorded. A background titration of buffer added to ANS-bound ALBP was subtracted from the salt displacement data. The data were fit with a simple inverse isotherm,

$$Y_I = \{[KCl]/IC_{50}\}/\{1 + [KCl]/IC_{50}\} \quad \text{(Eq. 4)}$$

where Y_I is the normalized fluorescence, and IC_{50} is the concentration of salt at 50% inhibition.

Stopped Flow Kinetic Analysis of ANS Binding to ALBP—Kinetics experiments were performed using a Biologic SF3 stopped flow interfaced with an ISS fluorometer. ALBP and ANS were rapidly mixed, and ANS fluorescence was monitored with excitation at 369 nm and emission at 470 nm. The assay buffer was 10 mM potassium phosphate, pH 7.5, 1% ethanol, and either 50 mM KCl or 1 M KCl. The resulting kinetic association curves were fit to the single exponential equation,

$$F = (F_{max} - F_0)\cdot(1 - e^{-k_{obs}(t - t_{offset})}) + F_0 \quad \text{(Eq. 5)}$$

where F is the fluorescence (dependent variable), $(F_{max} - F_0)$ is the amplitude of the transition, k_{obs} is the time constant of association, t is the time after the completion of injection (independent variable), t_{offset} is the x axis offset, which accounts for mixing time and the dead time of the instrument, F_0 is the initial fluorescence before binding, and F_{max} is the maximum fluorescence upon completion of binding. All parameters were allowed to float except F_0, which was determined by observing the fluorescence of ANS in buffer and was then fixed during fitting. The association of ANS with ALBP is very fast, so experiments were conducted at 6 °C to minimize loss of data during the dead time (~3 ms). For each concentration of ANS + ALBP, 5–12 shots over two different time scales (100 ms and 1 s) were averaged and collated. Using this technique, ~50% of the full extent of reaction can be captured (less for faster processes, more for slower processes), which affords excellent precision in the determination of k_{obs}. Determined rates are not affected

by the collection time scale, but averaging and obtaining high density overlapping data throughout the complete course of the reaction significantly improves the precision of the fits. Kinetic curves were fit to both single and double exponential functions with the result that all kinetic curves were judged to be single exponential curves. It should be noted that the sensitivity of ALBP to storage conditions, described under "ANS Binding," also appears to pertain to the kinetic behavior of the protein. Carefully handled and stored protein consistently produced well behaved single exponential kinetic curves.

For determination of the association (k_{on}) and dissociation (k_{off}) rate constants, the relaxation time constants were plotted as a function of the sum of the equilibrium concentrations of ANS plus ALBP (28). Equilibrium concentrations of ANS and ALBP were determined by an iterative fitting process (28). Briefly, $1/\tau$ ($1/\tau = k_{obs}$) is first plotted as a function of total [ANS], and the ratio between the intercept (k_{off}) and the slope (k_{on}) of this plot is used to calculate a dissociation constant ($K_d = k_{off}/k_{on}$). This preliminary K_d is used along with the known total concentrations of ANS and ALBP in each sample to calculate new equilibrium concentrations for ANS and ALBP, which are then used to generate a new plot of $1/\tau$ *versus* [ANS]eq + [ALBP]eq. Seven to ten iterations of this procedure were sufficient to achieve excellent convergence.

Analytical Ultracentrifugation—Sedimentation equilibrium experiments were performed in 10 mM potassium phosphate, pH 7.5, at low (50 mM) and high (1 M) KCl concentrations, in a Beckman Optima XL-A analytical ultracentrifuge. The sample and reference sectors of Epon charcoal-filled double-sector cells were loaded, respectively, with 110 μl of unligated or ANS-bound ALBP in low or high salt buffer and 125 μl of the corresponding buffer. For the runs in the presence of ANS, the reference sector also contained ANS, the ANS concentration was ~100 μM, and the samples contained 1% ethanol. Runs were performed at 20 °C and 25,000 rpm for ~24 h. Absorbance was measured at 279 nm for unligated ALBP and 281 nm for ANS-bound ALBP. The ALBP concentration was 0.2 mg/ml. Data were analyzed using the Origin equilibrium analysis program in the Beckman analysis software package. Values of the partial specific volume of ALBP and the densities of the buffer solutions at 20 °C were calculated using the computer program SEDNTERP (available on the World Wide Web at biochem.uthscsa.edu/auc/software). Fitting data to models of higher oligomeric complexity did not reveal any contaminants or additional equilibria and confirmed that the data depict an ideal single species in solution.

RESULTS

Salt Significantly Stabilizes ALBP—Native ALBP displays a CD spectrum typical of a protein predominantly consisting of β-sheet. Fig. 2*A* shows the change in the CD spectrum as urea unfolds the protein. The largest spectral changes occur in the β-sheet trough around 217 nm, so for each denaturation the signals at wavelengths of 216, 217, and 218 nm were individually analyzed and averaged to obtain values for $\Delta G_{unfolding}$ as described under "Experimental Procedures." Fig. 2*B* shows representative denaturation curves for ALBP in different solution conditions. Urea denaturations of apo-ALBP at 25 °C as a function of added KCl reveal a significant (3 kcal/mol) salt-induced stabilization of the protein as the salt concentration is increased from 0 to 2 M (Table I). The salt stabilization effect on apo-ALBP appears to be mostly saturated at KCl concentrations above 250 mM. Measurements of the $\Delta G_{unfolding}$ at 37 °C in the presence and absence of 2 M KCl also show a significant (5.1 kcal/mol) salt-induced stabilization of ALBP. Thus, at 37 °C, the addition of 2 M salt more than doubles the stability of the protein. This is an extremely large salt-induced protein stabilization.

Salt Appears to Destabilize Lipid-bound ALBP—In contrast to the effect of salt on apo-ALBP, ANS-bound ALBP appears to be destabilized by KCl. At 0 mM KCl, ANS-bound ALBP has a free energy of unfolding of 9.7 kcal/mol. Additional stabilization relative to the apoprotein is expected from the contribution of the ANS binding energy. The binding of any ligand to a protein will stabilize it. However, instead of exhibiting a pattern of stabilization paralleling the apoprotein (offset by the added $\Delta G_{binding}$ of ANS), the holoprotein appears to become destabilized as salt is added. In general, the denaturation curves are less well behaved at high ANS concentrations, and this leads to higher propagated errors on the determined free energies. This situation results in significant overlap of the fitted $\Delta G_{unfolding}$ values in the presence of bound ANS (Table I). However, although the error envelopes overlap, the low salt data cannot be fit using the high salt value of $\Delta G_{unfolding}$ (6.8 kcal/mol), and the high salt data cannot be fit using the low salt value of $\Delta G_{unfolding}$ (9.7 kcal/mol). Furthermore, the data clearly and

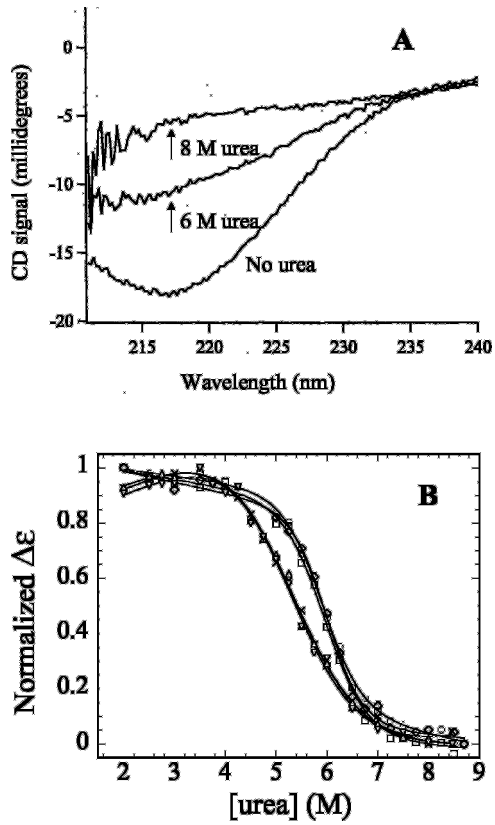

FIG. 2. **Chemical denaturations of apo- and ANS-bound ALBP.** *A*, raw CD spectra of ALBP at increasing urea concentrations. Like those of most predominantly β-sheet proteins, the CD spectrum of native ALBP has a trough near 217 nm. The CD spectra of ALBP are shown at 0, 6, and 8 M urea in 10 mM potassium phosphate, 50 mM KCl, pH 7.5. Note the loss of CD signal intensity with added urea, indicative of a loss of secondary structure and unfolding of the protein. *B*, representative urea-induced chemical denaturations of apo-ALBP (*leftmost set* of *curves*, *triangles*, *inverted triangles*, and *crosses*) and ANS-bound ALBP (*rightmost set* of *curves*, *squares*, *diamonds*, and *circles*), both at 50 mM KCl. Data were collected at 216, 217, and 218 nm for each experiment, and each *symbol* shows data for a particular wavelength. *Lines* through the data are best nonlinear fits to the linear extrapolation model (see "Experimental Procedures").

TABLE I
$\Delta G_{unfolding}$ of ALBP with increasing KCl (in kcal/mol)

Values are the average of 3-6 $\Delta G_{unfolding}$ values from individual curves monitored at 216, 217, and 218 nm and fit with Equation 1 as described under "Experimental Procedures." All experiments were performed in 10 mM potassium phosphate buffer, pH 7.5, at the indicated temperatures with the indicated amounts of added KCl.

[KCl]	apo-ALBP, 25 °C	apo-ALBP, 37 °C	ANS-bound ALBP, 25 °C[a]
mM			
0	4.8 ± 0.8	4.0 ± 1.0	9.7 ± 2.0
50	4.8 ± 0.6		8.7 ± 1.1
250	6.8 ± 0.7		7.1 ± 1.0
500	6.7 ± 0.7		6.7 ± 0.9
1000	6.7 ± 0.4		6.8 ± 0.7
2000	7.8 ± 0.9	9.1 ± 1.4	

[a] In all ANS-bound ALBP denaturations, the concentration of ANS was 100 μM.

statistically significantly indicate that unlike the case for apo-ALBP, the $\Delta G_{unfolding}$ for holo-ALBP is not increasing with added salt. As discussed below, direct lipid binding experiments were conducted, which demonstrate that a major source (but not the sole source) of this effect is the salt-induced displacement of ANS from the protein. Thermodynamic linkage calculations indicate that this effect is coupled with a salt-induced increase of the affinity of ANS for the denatured state of ALBP. The combination of these two effects produces the observed results and results in the observed convergence of the stabilization energies for the apo- and holoproteins at higher salt concentrations (see "Thermodynamic Linkages among Stability, Ligand Binding, and Salt").

All of the unfolding data fit well to a two-state denaturation model (Equation 1). It is, however, possible that the observed stabilization is the result of a salt-induced shift between a two-state unfolding process and a three-state unfolding process (which would have a lower apparent $\Delta G_{unfolding}$ when analyzed as a two-state process). If this were true, however, the shift for the apoprotein would have to be three-state to two-state with added salt, whereas the shift for holoprotein would have to be two-state to three-state.

Salt Inhibits Lipid Binding to ALBP and Causes Lipid Release—Equilibrium binding of ANS to ALBP was measured using the intrinsic fluorescence increase of ANS upon binding. ANS binds specifically in the lipid binding cavity of ALBP (4, 8) and competes directly with the binding of other lipids (7). Fig. 3*A* shows representative titrations at different KCl concentrations. Binding as a function of increased salt reveals that KCl weakens the association between ANS and ALBP. The K_d of ANS binding to ALBP increases from 0.48 to 4.4 μM upon increasing the KCl concentration from 50 to 750 mM (see Fig. 3 and Table II).

A thermodynamic linkage analysis of these data is also shown in Fig. 3. The slope of a plot of ln [salt] *versus* ln($1/K_d$) provides an estimate of the net uptake or displacement of ions upon ligand binding (26, 27). Fig. 3 shows that there exists a thermodynamic linkage of ~0.8 ions released upon binding of ANS. In other words, ANS binding causes the dissociation of essentially one monovalent ion from ALBP. Since thermodynamic linkages must be reciprocal, adding salt to holo-ALBP must also displace bound ligand. The salt-induced dissociation of ANS from ALBP was confirmed by titrating KCl into ANS-bound ALBP and observing the concomitant loss of fluorescence as the ANS dissociated (Fig. 3*C*). Note that ANS still binds to ALBP at high salt (Table II and data not shown), so Fig. 3*C* does not represent 100% displacement of ANS from the protein but shows a salt-induced equilibrium shift at one concentration of ANS. Analysis of the salt-induced displacement of ANS with a simple inverse isotherm (Equation 2), representing competitive inhibition, yields an IC_{50} value of 172 mM KCl.

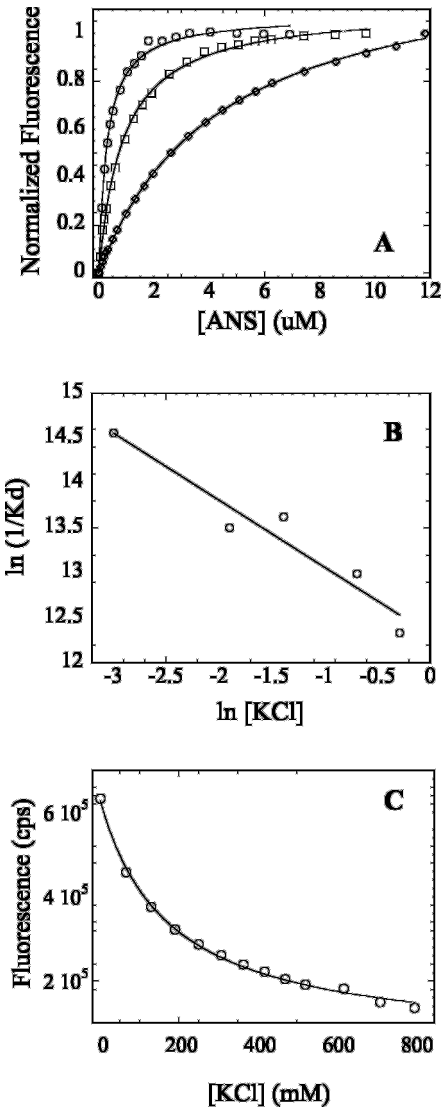

FIG. 3. **Dependence of ANS-ALBP binding on salt.** *A*, shown are representative equilibrium binding titrations monitoring the normalized change in fluorescence upon binding of ANS to ALBP in the presence of 50 mM (*circles*), 250 mM (*squares*), and 750 mM (*diamonds*) KCl. *B*, linkage plot of the relationship between ANS binding and KCl concentration. The slope of approximately −0.8 calculated from this plot suggests the release of one monovalent ion upon the binding of one ANS, and *vice versa*. *C*, salt-induced dissociation of ANS from ALBP. Concentrated KCl (4 M) in 10 mM potassium phosphate at pH 7.5 was titrated into 0.05 μM ALBP and 5.5 μM ANS. The addition of KCl causes the dissociation of ANS from ALBP and a concomitant loss of fluorescence. The line fit through the data is a simple inverse isotherm (see "Experimental Procedures").

Salt Effects on the Kinetics of ANS-ALBP Binding—The kinetics of ANS association with ALBP were monitored by stopped flow fluorescence spectroscopy over a range of ANS concentrations at 50 mM and 1 M KCl. Fig. 4*A* shows representative kinetic curves at low and high salt concentrations along with fits of the data to single exponential equations. Since the mixing of ANS and ALBP is essentially a relaxation toward equilibrium, the observed kinetic process will include contributions from both the association (k_{on}) and dissociation (k_{off}) reactions. Relaxation kinetic processes display exponential progress toward equilibrium, and analysis of the resulting time constants as a function of differing concentrations of reactants is used to determine the k_{on} and k_{off} constants for the reaction.

The values of $1/\tau$ for the association of ANS and ALBP are plotted as a function of the sum of the equilibrium concentrations of ANS and ALBP in Fig. 4*B* for both low and high salt. The slopes of these plots yield the k_{on}, whereas the intercepts provide k_{off} (28). Both the on and off rates are altered by salt, and the determined rate constants are reported in Table III. The addition of salt slows down the association of ANS with ALBP by more than 50% and speeds up the dissociation of ANS from ALBP by almost 3-fold. The quantitative determination of k_{off} in the rapid mixing experiments exhibits lower precision (higher error) largely because the on-rate dominates the observed relaxation at experimentally accessible reactant concentrations, but it can be clearly seen in Fig. 4*B* that the intercept of k_{obs} *versus* $1/\tau$ (which determines k_{off}) is certainly larger at 1 M KCl than at 50 mM, indicating a salt-induced increased off rate.

The association of ANS with ALBP is quite fast, possibly

TABLE II
ANS-ALBP binding as a function of KCl

Values are from fits to Equation 2 as described under "Experimental Procedures." Reported values at 150, 500, and 750 mM KCl are from single titrations, and values at 50 and 250 mM KCl are averages from six and three-titrations, respectively; however, this entire series was replicated several times with essentially identical results (data not shown). All experiments were performed at 25 °C, in 10 mM potassium phosphate buffer, pH 7.5, with the indicated amount of potassium chloride.

[KCl]	K_d	ΔG
mM	*μM*	*kcal/mol*
50	0.48 ± 0.14	8.62 ± 2.54
150	1.37 ± 0.05	7.99 ± 0.29
250	1.21 ± 0.43	8.07 ± 2.88
500	2.27 ± 0.20	7.69 ± 0.67
750	4.40 ± 0.07	7.30 ± 0.12

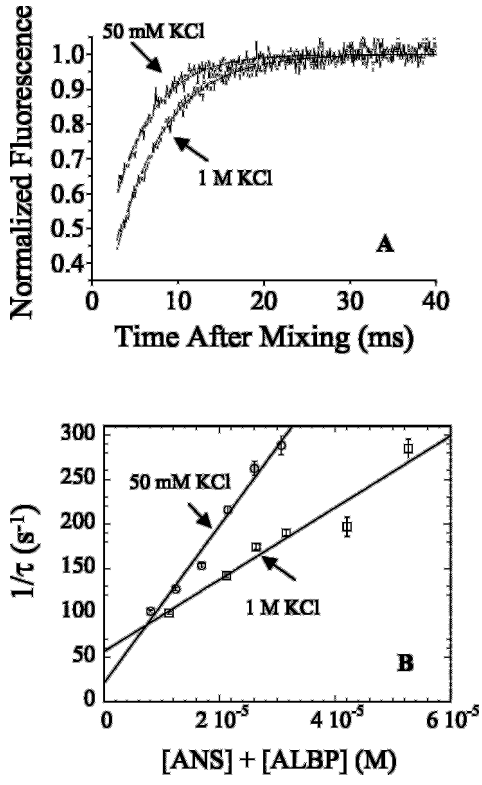

FIG. 4. **Salt effects on the kinetics of ANS-ALBP binding.** *A*, representative curves showing the increase in fluorescence with time as ANS associates with ALBP. Experiments were performed in 10 mM potassium phosphate, pH 7.5, at 50 mM and 1 M KCl. The ANS concentrations for the curves shown were 23.4 μM (50 mM KCl) and 27.1 μM (1 M KCl). To obtain a sufficient density of data points on short and long time scales, data were collected for 100- and 1000-ms durations. The resulting exponential curves were averaged and collated before analysis; thus, each kinetic constant represents a fit of 5–12 data sets. The fluorescence change has been normalized, and time 0 depicts the time of completion of injection/mixing. *B*, this plot shows the reciprocals of the observed time constants for ALBP-ANS association as a function of the sum of the equilibrium concentrations of ANS plus ALBP. The plot was generated as described under "Experimental Procedures." The slopes of these dependences yield k_{on}, and the *y* intercepts are k_{off}. Note that as [KCl] increases, the on-rate decreases and the off-rate increases.

even diffusion-controlled. Thus, in order to capture a significant portion of the kinetic process, all of the kinetics measurements were performed at 6 °C. Accordingly, it can be seen that the K_d values for binding of ANS to ALBP calculated from the k_{off}/k_{on} ratios at 6 °C (Table III) are higher than those determined by direct binding at 25 °C (Table II) but that the same reduction in binding affinity with added KCl occurs at both temperatures. The decrease in binding affinity with decreased

TABLE III
Kinetics of ANS binding to ALBP at low and high salt

The top portion shows fitted time constants (k_{obs}) for the association of ANS with ALBP at different reactant concentrations. Values are the results of fits of a single exponential to averaged data from 5–12 replicates. The concentration of ALBP was held constant at 2.5 μM. All experiments were carried out at 6 °C in 10 mM potassium phosphate buffer, pH 7.5, with either 50 mM or 1 M potassium chloride. The bottom portion shows correspondingly determined values of k_{on} and k_{off} (as described under "Experimental Procedures") and K_d for ANS binding at high and low salt ($K_d = k_{off}/k_{on}$).

50 mM KCl		1 M KCl	
[ANS]	k_{obs}	[ANS]	k_{obs}
μM	s^{-1}	*μM*	s^{-1}
9.38	102 ± 1	10.8	99 ± 1
14.1	127 ± 2	21.7	142 ± 2
18.8	153 ± 2	27.1	174 ± 3
23.4	216 ± 4	32.5	190 ± 4
28.1	263 ± 8	43.3	197 ± 11
32.8	288 ± 10	54.2	285 ± 11
k_{on} (s^{-1} M^{-1})	$8.9 \pm 0.6 \times 10^6$	k_{on} (s^{-1} M^{-1})	$4.0 \pm 0.5 \times 10^6$
k_{off} (s^{-1})	21 ± 13	k_{off} (s^{-1})	56 ± 18
K_d (μM)	2.3	K_d (μM)	14

temperature in this temperature range is consistent with previous observations (8). Although ANS binds to ALBP with negative enthalpy (8), there is a negative heat capacity change (ΔCp) upon binding (8), which results in curvature of the van't Hoff plot for ANS binding, such that affinity will increase with temperature at lower temperatures and then will decrease with temperature at higher temperatures.

Salt Stabilization of ALBP Is Not Linked to Protein Oligomerization—Salt-induced oligomerization of ALBP would be one of the simplest molecular mechanisms that could potentially account for the relatively large stabilization of ALBP by salt. Formation of dimers or higher order oligomers of any protein would result in a higher apparent $\Delta G_{unfolding}$ due to the additional stabilization free energy from the protein-protein interactions in the oligomer. Sedimentation equilibrium centrifugation is one of the most sensitive and reliable methods for detecting oligomerization of proteins. Fig. 5 shows sedimentation equilibrium profiles for ALBP in 50 mM and 1 M KCl. Both profiles reflect a well behaved monomeric protein. Parallel experiments in the presence of 100 μM ANS (data not shown) contained more noise in the data due to the ANS but also fit a single species of monomeric molecular weight. The amino acid sequence based molecular weight of ALBP is 14,578. The mean molecular weight returned by all four sedimentation equilibrium experiments (50 mM KCl with or without ANS and 1 M KCl with or without ANS) was 14,976 ± 7%. These data clearly demonstrate that there is not an oligomerization reaction linked to the lipid-binding or KCl-induced effects on ALBP.

DISCUSSION

We have demonstrated that KCl alters the stability, the ANS binding equilibrium, and the ANS binding kinetics of ALBP. Below, we discuss the thermodynamic linkages among these effects, potential molecular origins of these effects, and potential intracellular consequences of these effects.

Thermodynamic Linkages among Stability, Ligand Binding, and Salt—Fig. 6 illustrates the energetic linkages among ALBP stability, ANS binding to ALBP, and salt effects on ALBP as a thermodynamic cube. The front face of this cube depicts the stability and ANS binding equilibria for ALBP in the absence of excess salt: ΔG_1 is the folding/unfolding of apo-ALBP, ΔG_2 is the binding of ANS to ALBP, ΔG_3 is the folding/unfolding of ALBP with ANS bound, and ΔG_4 is the binding of ANS to the denatured state of ALBP. The back face of this

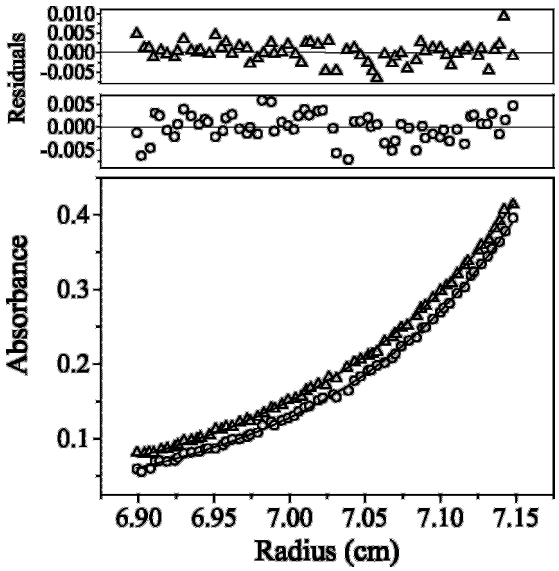

FIG. 5. **ALBP is monomeric at low and high salt concentrations.** Concentration distributions at sedimentation equilibrium during analytical ultracentrifugation are shown for ALBP at 50 mM (*circles*) and 1 M (*triangles*) KCl concentrations. *Lines* through the data show the fits to the concentration distribution of a monomeric, ideal particle at sedimentation equilibrium. The *upper panels* show the residuals of the fits for the two experiments.

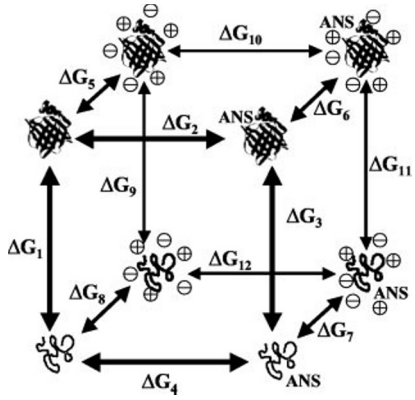

FIG. 6. **Thermodynamic linkages among unfolding, ANS binding, and the effects of salt on ALBP.** Each *reciprocal arrow* represents an equilibrium process such as binding or unfolding. The front face of the cube (with *boldface arrows*) is ALBP at low salt, and the far face of the cube (with *thinner arrows*) is ALBP at higher salt. The *right face* of the cube is ALBP with ANS bound, and the *left face* is ALBP without ANS bound. The *top face* shows ANS and KCl binding to the native state of ALBP, and the *bottom face* shows ANS and KCl binding to the denatured state of ALBP.

thermodynamic cube represents these same four equilibria in the presence of added salt (ΔG_9, ΔG_{10}, ΔG_{11}, ΔG_{12}). The remaining four free energies connecting the front and back faces of the cube correspond to the energetic consequences of adding salt to the native apo- and holo-ALBP molecules (ΔG_5, ΔG_6), and the denatured apo- and holo-ALBP molecules (ΔG_8, ΔG_7).

This thermodynamic cube thus illustrates the energetic relationships among stability, lipid binding, and salt effects that govern the structural and functional status of ALBP under any particular combination of these parameters. Furthermore, these thermodynamic relationships can be used to calculate the values of energetic parameters that have not or cannot be directly measured. For example, at any particular salt concentration, the depicted thermodynamic linkage can be used to calculate the free energy of binding of ANS to the denatured state of ALBP. At 50 mM KCl, the value of ΔG_4 (dissociation of ANS from the denatured state) is 4.7 kcal/mol ($\Delta G_1 + \Delta G_2 - \Delta G_3$ = 4.8 kcal/mol + 8.6 kcal/mol − 8.7 kcal/mol). Defined in the binding direction, the $\Delta G_{association}$ of ANS to the denatured state at 50 mM will therefore be −4.7 kcal/mol. This calculation provides the total free energy of binding of ANS to the denatured state as determined by conservation of energy but does not provide information on the stoichiometry of the reaction.

This calculation of the energy of ANS binding to the denatured state illustrates why binding of ANS to ALBP at 50 mM KCl does not appear to stabilize the native state of the protein as much as would be expected. Conservation of energy dictates that the binding of any ligand to a protein will increase its stability (29). ANS binding to ALBP at 50 mM KCl should stabilize the protein by an additional 8.6 kcal/mol (its dissociation free energy). However, because ANS also binds to the denatured state of ALBP, the stabilities of both the denatured and native states have been increased. Due to ANS binding, the denatured state is stabilized by 4.7 kcal/mol, and the native state is stabilized by 8.6 kcal/mol, yielding a difference between them of 3.9 kcal/mol.

Similar calculations can be performed at higher salt, with interesting conclusions. For example, at 500 mM KCl, the value of ΔG_{12} (dissociation of ANS from the denatured state) is calculated to be 7.7 kcal/mol ($\Delta G_9 + \Delta G_{10} - \Delta G_{11}$ = 6.7 kcal/mol + 7.7 kcal/mol − 6.7 kcal/mol). The $\Delta G_{association}$ of ANS to the denatured state at 500 mM salt is therefore −7.7 kcal/mol. Thus, notably, thermodynamic linkage shows that increased salt will increase the affinity of ANS for the denatured state of ALBP. This suggests that binding of ANS to the denatured state of ALBP is dominated by hydrophobic interactions. Furthermore, this calculation explains the unusual finding that the unfolding free energies of apo-ALBP and holo-ALBP essentially converge at high salt (see Table I). This convergence is unexpected at first, again because conservation of energy dictates that ANS binding to ALBP will increase its stability, and ANS still binds to native ALBP with micromolar affinity even at high salt concentrations. Thus, one would normally expect the lipid-bound protein to always have a higher free energy of unfolding than the apoprotein, even at high salt. However, at high salt, the affinities of ANS for the native and the denatured forms of ALBP are calculated via the thermodynamic linkage to be essentially equal. This means that binding of ANS at high salt will not preferentially stabilize either state of the protein. Thus, although ANS is binding to ALBP at high salt, the net effect of ANS binding on stabilization disappears, and the stabilization free energies of the apo- and holo-forms of the protein converge at high salt.

These thermodynamic relationships are dictated by mass and energy balance and are effectively "model-independent." In other words, whereas we discuss several potential molecular mechanisms for the action of salt below, the thermodynamic relationships shown in Fig. 6 and discussed above will hold regardless of the particular molecular mechanism producing these effects. The characterization of the binding of ANS to the denatured states of ALBP discussed above is one of the first quantitative determinations of the binding free energy of ANS to the denatured state of any protein.

Potential Molecular Origins of the Effects of Salt on ALBP—Added salts have long been known to have both stabilizing and destabilizing effects on many proteins (30–37). The magnitude of the salt stabilization of ALBP observed herein is on the high side of salt-induced protein stabilization effects. A number of molecular mechanisms have been proposed to explain the effects of salt on protein stability, including preferential hydration, specific ion binding, and electrostatic screening of surface charge repulsions (30–37); however, clear assignment of the origins of a salt-induced effect to a particular molecular model

has only been accomplished for a few well characterized systems. Relative to stability studies, far fewer studies of the salt effects on ligand binding to proteins have been performed, with the notable exception of DNA-binding proteins, where characterization of the salt dependence of binding is usually one of the first and primary empirical characteristics examined. In contrast, investigations of the salt effects on the binding of lipids to proteins are scarce.

Molecular models for explaining the effects of added salt on protein stability and function can be divided into several categories. Salt effects may be general (independent of the ion type) or ion-specific. In addition, such general or specific salt effects may be manifested via effects of the salt on the solvent environment, or they may involve direct ion binding to the protein. Furthermore, the effects of salt on ligand binding in particular may involve direct competitive inhibition due to ion binding in the active site, or indirect long range allosteric effects due to ion binding at a remote site or sites. The current data for ALBP, while demonstrating salt-induced modulation of the stability and function of the protein, afford only initial discussion of possible molecular origins for these effects.

One general model consistent with the current results for ALBP is charge screening. Any time two charged molecules interact in a solution containing added salt, the tendency of solvent ions to surround and screen the two interacting molecules effectively reduces their effects upon each other. Thus, the electrostatic attraction between ANS and ALBP would be reduced and could account for the reduction of binding affinity in the presence of increased salt. Effects of salt on stability can similarly be explained as a screening of repulsive interactions. The electrostatic topology of ALBP, as seen in Fig. 1, shows that large patches or clusters of like charge occur on the surface of the protein. As has been proposed by Fink and associates (33, 37), added salt would screen the repulsive interactions within each extended patch and thus stabilize the protein.

Conformational tightening or constriction of a protein's structure has been proposed in other systems to explain the effects of salt and ANS on the stability of some proteins (38). At first glance, such a mechanism might seem applicable to the data on ALBP. It is known that conformational flexibility is required for the binding of lipids to ALBP (4). Structural studies of ALBP have shown that whereas there is a large stable lipid binding cavity both in the presence and absence of bound lipid, there is no stable access channel to this cavity (4). Thus, the protein must conformationally flex in order for lipids to enter and leave the cavity. Salt-induced conformational tightening of ALBP could both stabilize the protein and reduce lipid binding affinity. However, the kinetics of lipid binding and release determined in this study rule out this attractive model. Restriction of structural mobility would make it more difficult for lipids to both enter and leave the cavity. However, the data in Fig. 4 and Table III show that in the presence of added salt, the association rate for ANS binding is reduced, but the dissociation rate is increased. This is a somewhat simplistic projection of the potential functional consequences of conformational tightening, however. Furthermore, determinations of kinetic constants such as k_{off} are always kinetic mechanism-dependent, and whereas the kinetic data in this study are well described by a simple relaxation mechanism, the situation could be more complicated. Thus, whereas the salt effects on k_{off} as presented appear to rule out conformational tightening, further exploration of this model may still be warranted.

Along with charge screening, discussed above, another major molecular model that would be consistent with all of the current data for ALBP is a specific ion binding event. The nearly 1:1 reciprocal linkage between salt and ANS binding (Fig. 3) suggests such a model. If the salt-induced stabilization of the protein is similarly analyzed as a thermodynamic linkage using Equation 3 as described under "Experimental Procedures" (analysis not shown), it suggests an uptake of between 0.6 and 1.0 ions upon stabilization of ALBP by salt. It is possible that direct ion binding could both stabilize the protein and compete directly with ANS for binding to the protein. The most extreme form of this model would be the simultaneous stabilization of the protein and reduction of lipid binding affinity via the binding of a single ion to a single site on the protein.

The investigation of the effects of different salts on a protein and the site-directed mutation of potential ion binding sites are two approaches to determining whether salt effects are ion-specific or general and are two foci of future studies in our laboratory. Preliminary results suggest that the thermodynamic linkage between salt and ANS binding does change somewhat with salts other than KCl (work in progress), suggesting that the modulation of ANS binding does have some ion-specific character. Ion-specific binding and general charge screening are not mutually exclusive mechanisms, and both may be involved in the salt modulation of the stability and function of ALBP. The data in this study, however, indicate that conformational tightening and linked higher order oligomerization are not involved in manifestation of the salt regulation of ALBP. Much of this discussion has to some extent effectively assumed that the underlying mechanisms for the salt effects on stability and lipid binding are the same or overlap at the molecular level, and this may not be the case. It is certainly possible that the two effects, while thermodynamically linked, do not share the same molecular origins.

Potential in Vivo Consequences of the Salt Regulation of ALBP—The effects of KCl on the stability and lipid binding affinity of ALBP have been examined across wide concentration ranges in order to help definitively establish and quantitate these effects. These data show, however, that these effects will occur under physiological salt conditions. Within the cell, ALBP will have higher stability and lower lipid affinity than would be predicted from previously reported *in vitro* studies. Furthermore, the midpoints of the salt effects on both stability and lipid binding are near physiological salt concentrations. The IC_{50} for the salt displacement of ANS from ALBP is 172 mM (Fig. 3). The major portion of the salt stabilization of ALBP occurs between 50 and 250 mM KCl (Table I). The normal intracellular concentration of potassium is ~139 mM (39, 40). The midpoints of these effects are where they will be highly sensitive to salt modulation. This means that small changes in the physiological salt concentration will directly regulate the activity and structural stability of ALBP. Decreases in intracellular potassium concentrations of 18% have been linked to type 2 diabetes (40).

In an elegant series of studies, Storch and associates have demonstrated that ALBP transfers fluorescent fatty acids to lipid membranes via a direct collisional mechanism (11–13). Salt effects on the transfer rate of fluorescent fatty acids from ALBP to lipid vesicles have been used as one of many criteria for postulating the direct interactions between ALBP and lipid vesicles. Whereas many other avenues of evidence have been used to demonstrate these direct interactions, the salt-induced release of bound lipid demonstrated in Fig. 3 and the salt effects on the kinetics of lipid binding shown in Fig. 4 indicate that salt effects in lipid transfer assays may not unequivocally be used as a sole indicator of the existence of collisional donor-acceptor interactions with ALBP.

Linkages among salt, hypertension, and insulin resistance have been noted for many years in diabetes research (*e.g.* Refs. 41 and 42), including linkages to fatty acid metabolism (43).

ALBP itself has been directly linked to obesity, diabetes, and atherosclerosis (6, 44, 45). ALBP has been shown to localize to the nucleus in the early stages of adipocyte differentiation (46) and in response to cellular uptake of certain nuclear hormone receptor ligands (47). In the nucleus, ALBP interacts directly or indirectly with peroxisome proliferator-activated receptor γ (PPARγ) (47, 48). PPARγ is a nuclear hormone receptor that is activated by fatty acids and other intracellular lipids (49). PPARγ controls adipocyte differentiation, including the direct transcriptional regulation of ALBP expression (for reviews, see *e.g.* Refs. 50 and 51). Depending on the circumstances and the particular lipid involved, ALBP can apparently either deliver activating lipids to PPARγ (47) or competitively deplete ligands from PPARγ (48).

Because salt regulates the lipid binding activity of ALBP, it would also regulate the transfer of lipids between ALBP and PPARγ in the nucleus. The existence of potassium gradients between the nucleus and the cytoplasm has recently been demonstrated in hepatocytes (52). Such gradients and the likely presence of higher overall amounts of salt in the nucleus relative to the cytoplasm due to the presence of electrostatically balancing counterions localized near DNA could have a definite impact on this important intracellular signaling interaction. One scenario might envision ALBP simply releasing some ligands upon entering the nucleus due to interactions with the differing ionic environment relative to the cytoplasm. As more studies emerge focusing on the electrostatic aspects of lipid-protein interactions, so should a more complete understanding of the balance between hydrophobic forces and electrostatic forces in controlling these important intracellular interactions.

REFERENCES

1. Banaszak, L., Winter, N., Xu, Z., Bernlohr, D. A., Cowan, S., and Jones, T. A. (1994) *Adv. Protein Chem.* **45,** 89–151
2. Bernlohr, D. A., Simpson, M. A., Hertzel, A. V., and Banaszak, L. J. (1997) *Annu. Rev. Nutr.* **17,** 277–303
3. Stewart, J. M. (2000) *Cell. Mol. Life Sci.* **57,** 1345–1359
4. Layne, M. D., Patel, A., Chen, Y.-H., Rebel, V. I., Carvajal, I. M., Pellacani, A., Ith, B., Zhao, D., Schreiber, B. M., Yet, S.-F., Lee, M.-E., Storch, J., and Perrella, M. A. (2001) *FASEB J.* **15,** 2733–2735
5. Perrella, M. A., Pellacani, A., Layne, M. D., Patel, A., Zhao, D., Schreiber, B. M., Storch, J., Feinberg, M. W., Hsieh, C. M., Haber, E., and Lee, M. E. (2001) *FASEB J.* **15,** 1774–1776
6. Hotamisligil, G. S., Johnson, R. S., Distel, R. J., Ellis, R., Papaioannou, V. E., and Spiegelman, B. M. (1996) *Science* **274,** 1377–1379
7. Kane, C. D., and Bernlohr, D. A. (1996) *Anal. Biochem.* **233,** 197–204
8. Ory, J. J., and Banszak, L. J. (1999) *Biophys. J.* **77,** 1107–1116
9. Nicholls, A., Sharp, K., and Honig, B. (1991) *Proteins* **11,** 281–296
10. LiCata, V. J., and Bernlohr, D. A. (1998) *Proteins* **33,** 577–589
11. Wootan, M. G., Bernlohr, D. A., and Storch, J. (1993) *Biochemistry* **32,** 8622–8627
12. Wootan, M. G., and Storch, J. (1994) *J. Biol. Chem.* **269,** 10517–10523
13. Smith, E. R., and Storch, J. (1999) *J. Biol. Chem.* **274,** 35325–35330
14. Jakoby, M. G., Miller, K. R., Toner, J. J., Bauman, A., Cheng, L., Li, E., and Cistola, D. P. (1993) *Biochemistry* **32,** 872–878
15. Kirk, W. R., Kurian, E., and Prendergast, F. G. (1996) *Biophys. J.* **70,** 69–83
16. Matulis D., and Lovrien R. (1998) *Biophys. J.* **74,** 422–429
17. Xu, Z., Buelt, M. K., Banaszak, L. J., and Bernlohor, D. A. (1991) *J. Biol. Chem.* **226,** 14367–14370
18. Simpson, M. A., and Bernlohr, D. A. (1998) *Biochemistry* **37,** 10980–10986
19. Matarese, V., and Bernlohr, D. A. (1988) *J. Biol. Chem.* **263,** 14544–14551
20. Pace, C. N. (1986) *Methods Enzymol.* **14,** 266–280
21. Johnson, W. C., Jr. (1988) *Annu. Rev. Biophys. Biophys. Chem.* **17,** 145–166
22. Santoro, M. M., and Bolen, D. W. (1988) *Biochemistry* **27,** 8063–8068
23. Heyduk, T., and Lee, J. C. (1990) *Proc. Natl. Acad. Sci. U. S. A.* **87,** 1744–1748
24. Inglese, J., Blatchly, R. A., and Benkovic, S. J. (1989) *J. Med. Chem.* **32,** 937–940
25. Datta, K., and LiCata, V. J. (2003) *J. Biol. Chem.* **278,** 5694–5701
26. Wyman, J. (1964) *Adv. Protein Chem.* **19,** 223–286
27. Lohman, T. M., and Mascotti, D. P. (1992) *Methods Enzymol.* **212,** 400–424
28. Bernasconi, C. F. (1976) *Relaxation Kinetics*, Academic Press, Inc., pp. 11–13, New York
29. Schellman, J. A. (1987) *Annu. Rev. Biophys. Biophys. Chem.* **16,** 115–137
30. von Hippel, P. H., and Schleich, T. (1969) in *Structure and Stability of Biological Macromolecules in Solution* (Timasheff, S. N., and Fasman, G. D., eds) pp. 417–574, Marcel Decker, Inc., New York
31. Schellman, J. A. (1987) *Biopolymers* **26,** 549–559
32. Pace, C. N., and Grimsley, G. R. (1988) *Biochemistry* **27,** 3242–3246
33. Goto, Y., Takahashi, N., and Fink, A. L (1990) *Biochemistry* **29,** 3480–3488
34. Arakawa, T., Bhat, R., and Timasheff, S. N. (1990) *Biochemistry* **29,** 1924–1931
35. Yang, A. S., and Honig, B. (1992) *Curr. Opin. Struct. Biol.* **2,** 40–45
36. Timasheff, S. N. (1995) *Methods Mol. Biol.* **40,** 253–269
37. Nishimura, C., Uversky, V. N., and Fink, A. L. (2001) *Biochemistry* **40,** 2113–2128
38. Matulis, D., Baumann, C. G., Bloomfield, V. A., and Lovrien, R. E. (1999) *Biopolymers* **49,** 451–458
39. Lodish, H. Berk, A., Zipursky, S. L., Matsudaira, P., Baltimore, D., and Darnell, J. (1999) in *Molecular Cell Biology*, 4th Ed., p. 585, W. H. Freeman and Co., New York
40. Resnick, L. M. Barbagallo, M., Dominguez, L. J., Veniero, J. M., Nicholson, J. P., and Gupta, R. K. (2001) *Hypertension* **38,** 709–712
41. Ferrannini, E., Buzzigoli, G., Bonadonna, R., Giorico, M. A., Oleggini, M., Graziadei, L., Pedrinelli, R., Brandi, L., and Bevilacqua, S. (1987) *N. Engl. J. Med.* **317,** 350–357
42. Ogihara, T., Asano, T., Ando, K., Chiba, Y., Sekine, N., Sakoda, H., Anai, M., Onishi, Y., Fujishiro, M., Ono, H., Shojima, N., Inukai, K., Fukushima, Y., Kikuchi, M., and Fujita, T. (2001) *Diabetes* **50,** 573–583
43. Donovan, D. S., Soloman, C. G., Seely, E. W., Williams, G. H., and Simonson, D. C. (1993) *Am. J. Physiol.* **264,** E730–E734
44. Makowski, L., Boord, J. B., Maeda, K., Babaev, V. R., Uysal, K. T., Morgan, M. A., Parker, R. A., Suttles, J., Fazio, S., Hotamisligil, G. S., and Linton, M. F. (2001) *Nat. Med.* **7,** 699–705
45. Berg, J. P. (1997) *Eur. J. Endocrinol.* **136,** 467–468
46. Helledie, T., Antonius, M., Sorenson, R. V., Hertzel, A. V., Bernlohr, D. A., Kolvraa, S., Kristiansen, K., and Mandrup, S. (2000) *J. Lipid Res.* **41,** 1740–1751
47. Tan, N. S., Shaw, N. S., Vinckenbosch, N., Liu, P., Yasmin, R., Desvergne, B., Wahli, W., and Noy, N. (2002) *Mol. Cell. Biol.* **22,** 5114–5127
48. Helledie, T., Jorgensen, C., Antonius, M., Krogsdam, A. M., Kratchmarova, I., Kristiansen, K., and Mandrup, S. (2002) *Mol. Cell Biochem.* **239,** 157–164
49. Kliewer, S. A., Sundseth, S. S., Jones, S. A., Brown, P. J., Wisely, G. B., Koble, C. S., Devchand, P., Wahli, W., Willson, T. M., Lenhard, J. M., and Lehmann, J. M. (1997) *Proc. Natl. Acad. Sci. U. S. A.* **94,** 4318–4323
50. Grimaldi, P. A. (2001)) *Prog. Lipid Res.* **40,** 269–281
51. Spiegelman, B. M. (1998) *Diabetes* **47,** 507–514
52. Garner, M. H. (2002) *J. Membrane Biol.* **187,** 97–115